Distribution of Glial-Associated Proteins in the Developing Chick Auditory Brainstem

Matthew J. Korn, Karina S. Cramer

Department of Neurobiology and Behavior, University of California at Irvine, Irvine, California 92697-4550

Received 29 December 2007; revised 15 March 2008; accepted 26 March 2008

ABSTRACT: **In the avian brainstem, nucleus magnocellularis (NM) projects bilaterally to nucleus laminaris (NL) in a pathway that facilitates sound localization. The distribution of glia during the development of this pathway has not previously been characterized. Radial glia, astrocytes, and oligodendrocytes facilitate many processes including axon pathfinding, synaptic development, and maturation. Here we determined the spatiotemporal expression patterns of glial cell types in embryonic development of the chick auditory brainstem using glial-specific antibodies and histological markers. We found that vimentin-positive processes are intercalated throughout the NL cell layer. Astrocytes are found in two domains: one in the ventral neuropil region and the other dorsolateral to NM. GFAP-positive processes are primarily distributed along the ventral margin of NL. Astrocytic processes penetrate the NL cell layer following the onset of synaptogenesis, but before pruning and maturation. The dynamic, nonoverlapping expression patterns of GFAP and vimentin suggest that distinct glial populations are found in dorsal versus ventral regions of NL. Myelination occurs after axons have reached their targets. FluoroMyelin and myelin basic protein (MBP) gradually increase along the mediolateral axis of NL starting at E10. Multiple GFAP-positive processes are directly apposed to NM-NL axons and MBP, which suggests a role in early myelinogenesis. Our results show considerable changes in glial development after initial NM-NL connections are made, suggesting that glia may facilitate maturation of the auditory circuit.** © 2008 Wiley Periodicals, Inc. Develop Neurobiol 68: 1093–1106, 2008

Keywords: **nucleus magnocellularis; nucleus laminaris; glia; vimentin; GFAP**

INTRODUCTION

Neuroglial interactions play an important role in the construction of neuronal circuitry. Radial glia facilitate the migrating of neurons and are responsible for the arrangement of laminae in the cortex (Rakic, 1978; Poluch and Juliano, 2007). In addition to maintaining the ionic environment at the synapse, astrocytes communicate via purinergic signaling to regulate synaptic strength (Bergles et al., 1999; Zhang et al., 2003; Pascual et al., 2005). Oligodendrocytes interact directly with axons during myelination and may be responsible for the inhibition of aberrant collaterals (Kapfhammer, 1997; Chen et al., 2002). The changes to glial populations in the injured or diseased brain underscore the importance of elucidating their function during development (Pekny and Pekna, 2004; Sandvig et al., 2004).

In the avian brainstem, VIIIth nerve axons contact neurons in nucleus magnocellularis (NM), which in turn, project bilaterally to nucleus laminaris (NL). NL is composed of a layer of neurons with bitufted dendritic arbors. Axon branches from NM neurons contact dorsal dendrites on the ipsilateral side and ventral dendrites on the contralateral side of NL. These differential projections, along with delay lines in the contralateral projection, allow NL neurons to

Correspondence to: K.S. Cramer (cramerk@uci.edu).

Contract grant sponsor: NIH; contract grant numbers: NIDCD 005771, NSF IOS-0642346, and NIH 5 T32 MH014599-29.

Published online 22 May 2008 in Wiley InterScience (www.interscience.wiley.com).
DOI 10.1002/dneu.20645

compute interaural time differences, which are used to determine the locations of sounds in space (Carr and Konishi, 1990; Overholt et al., 1992; Agmon-Snir et al., 1998). This pathway develops before auditory experience can influence growing axons (Young and Rubel, 1986) and it is not extensively refined until after the initial connections are made.

Previous studies have demonstrated that axon guidance molecules are expressed in the auditory periphery and brainstem, and that these molecules may aid in directing auditory brainstem axons to find their appropriate targets (Fritzsch et al., 1999; Tierney et al., 2001; Cramer, 2005; Webber and Raz, 2006; Howell et al., 2007; Huffman and Cramer, 2007). However, the cellular interactions that are responsible for establishing and maintaining these connections into maturity remain unclear. In this study, we determined the spatiotemporal distribution of proteins that represent specific glial populations. Using antibodies to vimentin, a putative radial glial protein, glial fibrillary acidic protein (GFAP), a predominantly astrocytic protein, and myelin basic protein (MBP), we examined a wide range of glial subtypes present in the auditory brainstem. We then evaluated the emergence of these non-neuronal cells in comparison to known events in chick auditory brainstem development.

The expression and distribution of these non-neuronal cells are consistent with a dynamic role for glia during the maturation of synapses in a newly developed circuit. We find that vimentin-positive glia and their processes are in close proximity with neurons during the latter stages of differentiation of NM and NL. The emergence of astrocytes coincides with changes in dendritic structure, consistent with a role in the development of synapses. Myelination occurs after axons have reached their targets during a time when the auditory pathway is functional. Together, these observations are consistent with the hypothesis that glia facilitate the development and maintenance of the auditory pathway.

METHODS

Animals

Fertilized eggs (AA Laboratories) were set in a rotating incubator at 39° and removed at ages E6-E19 (E6 = 2, E8 = 3, E10 = 7, E11 = 2, E12 = 2, E13 = 2, E14 = 6, E15 = 6, E16 = 4, E17 = 4, and E19 = 4).

Antibodies and Histology

For immunohistochemistry, brainstems were dissected in PBS, fixed for 2 h in 4% paraformaldehyde (PFA), and cryoprotected overnight in 30% sucrose. Protected brainstems were mounted in Tissue-Tek O.C.T. (Torrance, CA) and sectioned at 20 μm in the coronal plane using a Leica CM1850 cryostat. One in five sections was collected for immunolabeling or histology.

All sections were treated with an antigen retrieval step by rinsing with boiling PBS followed by a wash in 0.5% H_2O_2 in 100% methanol. Sections were blocked with normal goat serum or a blocking solution containing 5% nonfat dry milk and 0.1% Triton X-100 in PBS. Sections were incubated overnight in the following dilutions for each respective antibody; mouse monoclonal Vimentin (DAKO, 1:150), EphA4 (Soans et al., 1996, 1:300), rabbit polyclonal GFAP (pGFAP, DAKO, 1:300), mouse monoclonal GFAP (mGFAP, Sigma, 1:200), and rat monoclonal MBP (AbCam, 1:100). Alexa Fluor secondary antibodies were used at a 1:300 dilution.

In some cases, biotinylated secondary antibodies were used with a diaminobenzidine (DAB) peroxidase substrate or a Vectastain VIP Kit (Vector Laboratories). To detect myelin, sections were incubated in FluoroMyelin (FM, Molecular Probes, 1:300 in PBS) for 20 min and then rinsed thoroughly.

Sections were viewed on a Zeiss AxioSkop or Zeiss Pascal LSM 5 Confocal Microscope. Measurements were made using Zeiss OpenLab Software. Images were collected and edited using Jasc Photo Shop Pro 8 and Carl Zeiss LSM Image Browser.

Image Analysis

Quantitative analysis was performed on GFAP, MBP, and FM-labeled sections to determine how the distribution of labeled fibers within NL changes with age. We counted the number of labeled processes that penetrated into the NL cell layer in each section and averaged this value to obtain the mean number of fibers per section for each brain. We used the two-tailed Student's t test to compare means, and differences were considered statistically significant for p-values <0.05.

In Vitro Axon Labeling

Axon labeling was performed using *in vitro* labeling methods (Cramer et al., 2004, 2006; Burger et al., 2005a) to determine the proximity of glial markers to axons in the auditory circuit. E13–E15 chick embryos were removed from the egg, and the brainstems were immersed in oxygenated (95% O_2/5% CO_2) Tyrode's solution (8.12 g/L NaCl, 0.22 g/L KCl, 1.43 g/L $NaHCO_3$, 0.2 g/L $MgCl_2$, 0.333 g/L $CaCl_2$, and 22 g/L dextrose) for 30 min. A small bolus of rhodamine dextran amine (RDA; MW = 3000; Molecular Probes) was injected using a Picospritzer (Parker Instruments) into either NM or the midline. Injections into NM produced anterograde labeling of axons toward the dorsal side of the ipsilateral or the ventral side of the contralateral NL. Injections into the midline labeled ventral axons on both sides. RDA was used in a 6.25% solution containing

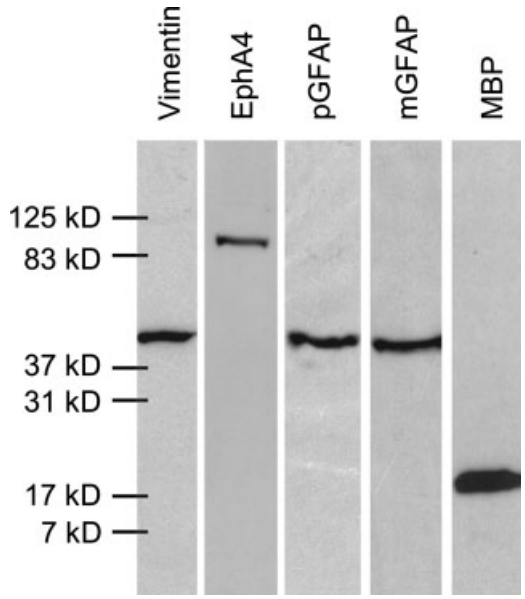

Figure 1 Western-blot analysis confirms specificity of all antibodies. A single band for vimentin is observed at 55 kDa. A single band for EphA4 at 109 kDa. A single band for GFAP is identified by the polyclonal GFAP (pGFAP) as well as the monoclonal GFAP (mGFAP) at 50 kDa, with the pGFAP appearing slightly larger. The antibody for MBP labels an intense band at 21 kDa. The density of the band may indicate that it includes trace levels of the 17 kDa isoform of MBP.

0.4% Triton X-100 in PBS. Following the injection of the dye, the brainstems were incubated for 2–3 h to allow for transport and then fixed in 4% PFA.

Western-Blot Analysis

We performed Western blots to ensure specificity of the antibodies used [see Fig. 1]. Three brainstems at each age were dissected on ice, homogenized, and assayed for protein concentration using a Bio-Rad D_C protein assay kit in conjunction with a SmartSpec Plus spectrometer (Bio-Rad, Hercules, CA).

Protein was run on a 12% Tris–HCl Ready Gel (Bio-Rad, Hercules, CA) and then transferred to a nitrocellulose membrane. Blots were then washed and incubated overnight with the antibodies in blocking solution containing 5% nonfat dry milk and 0.02% Tween in TBS. They were then rinsed and incubated with a horseradish peroxidase (HRP)-conjugated secondary antibody and visualized using the Immun-Star HRP Luminol/Enhancer system (Bio-Rad, Hercules, CA). Band size was verified using Bio-Rad Kaleidoscope prestained standards.

RESULTS

Although the neuronal changes that lead to the formation of precise auditory brainstem circuitry have been characterized, the role of glia in this process has not been explored. Here, we examined the expression of glial-associated proteins and described in detail the spatiotemporal pattern of cell types during the period of development coinciding with maturation of the auditory pathway.

At early ages (E6–E9), we evaluated the expression of vimentin at the level of the auditory anlage, a structure that contains precursors to NM and NL and is located in a dorsal and lateral position in the developing brainstem (Harkmark, 1954; Book and Morest, 1990; Cramer et al., 2000a). As the embryo matures (E10–E12), the anlage differentiates, giving rise to two distinctive nuclei, NM and NL, which lie in the dorsomedial brainstem.

At ages E10 and older, we describe the expression of vimentin, GFAP, FM, and MBP in relationship to NM and NL. NM contains large cells that exhibit endbulb synapses from VIIIth nerve afferents (Parks, 1981; Jhaveri and Morest, 1982; Carr, 1991). NL contains a layer of neurons whose dendrites extend into a cell-free neuropil region, which is bound by a distinctive glial margin (Rubel et al., 1976; Smith and Rubel, 1979). The glial cells that surround NL invade the neuropil region around E14, at which time NL displays cellular and dendritic reorganization (Smith, 1981). We focused on a region of the brainstem that includes the auditory brainstem nuclei throughout their rostrocaudal extent.

We first verified that our antibodies specifically recognized each protein using Western blots. Figure 1 shows that, in immunoblots, the antibodies only had bands corresponding to the appropriate size for each protein.

Vimentin and EphA4

Embryonic Days 6–8. Vimentin-positive processes extended from cell bodies located in the dorsal ventricular zone [Boxes in VZ in Fig. 2(A); see Inset 1 and 2] and extended an apical process, radially, to the ventral pial surface [Fig. 2(A,C)]. This pattern was prevalent throughout the entire extent of the brainstem. Numerous radially oriented vimentin-positive fibers spanned the entire dorsoventral extent of the brainstem.

The midline was intensely labeled and individual bundles of vimentin-positive processes were observed [Fig. 2(A–C)]. There were few processes in the area immediately lateral to the midline in the brainstem at E6 [Fig. 2(A)]. With exception to the auditory anlage, which was completely devoid of vimentin-positive processes, the lateral two-thirds of the brainstem con-

tained a dense network of fibers [Fig. 2(A,C)]. Brainstems from embryos aged E7 and younger contained densely labeled fascicles of radial processes in the more lateral regions of the brainstem [Fig. 2(A), black arrows; Fig. 2(B), white arrows]. These bundles were no longer observed after E8 [Fig. 2(C)].

The fiber pattern we observed at this age is reminiscent of the pattern we previously described for EphA4 (Cramer et al., 2000b). We thus performed double immunofluorescence to determine whether these vimentin-positive radial glial fibers express EphA4. We found that numerous processes coexpressed vimentin and EphA4 [Fig. 2(B)]. Double-labeled processes were most evident in the medial two-thirds of the brainstem. EphA4 expression was somewhat less intense in the more dorsal areas; therefore, the greatest association between the two expression patterns existed in close proximity to the ventral pial surface. This expression pattern suggests that EphA4 might mediate neuroglial interactions in this region of the brainstem.

Embryonic Days 10–16. By E10, the components of the auditory anlage have migrated medially, and both NM and NL can be distinguished morphologically [Fig. 2(D), white-dashed lines]. We observed a dense network of vimentin-positive processes in NM and NL [Fig. 2(D–F)]. In NM, processes were most evident in the dorsal half of the nucleus; however, several processes were observed within or just outside of the cell population. These vimentin-positive fibers were short (<30 μm) and appeared to originate from glial cell bodies located in the dorsal portion of the brainstem, in proximity to the VZ. Occasionally, lightly labeled radial fibers were observed along the axis of the VIth and VIIth cranial nerves (data not shown).

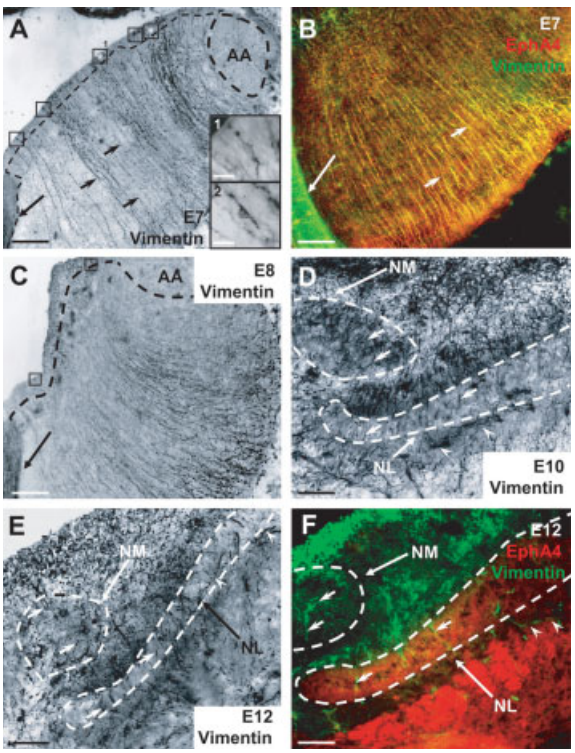

Figure 2

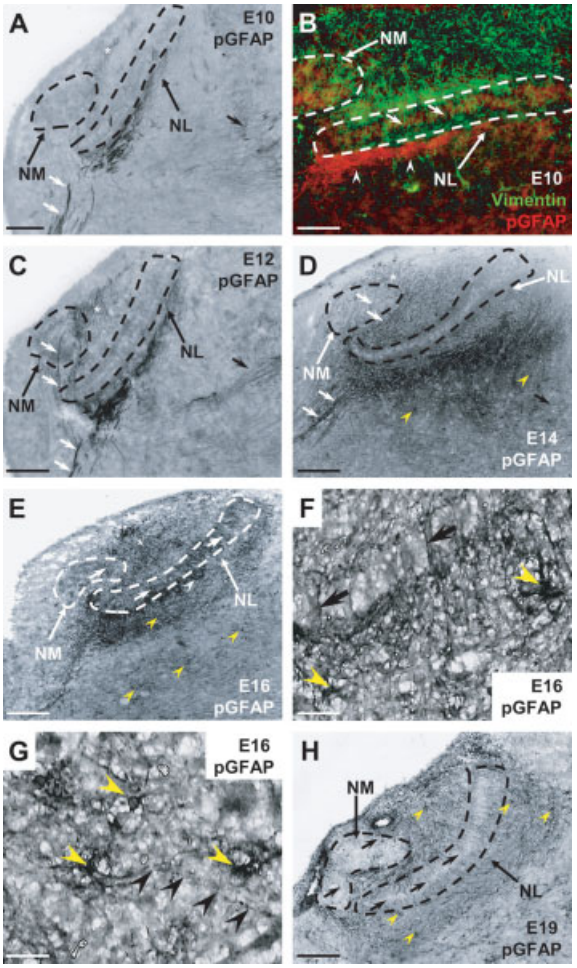

Figure 3

Vimentin-positive processes that crossed into NL originated from glia located outside the dorsal neuropil region of NL, along the glial margin [Fig. 2(D,F)]. In some cases, processes traversed the NL cell layer and into the ventral neuropil, but rarely did fibers pass beyond the ventral margin [Figs. 2(F) and 3(B)]. Fibers located proximal to the ventral glial margin coursed parallel to the mediolateral axis of NL [Fig. 2(D,E)]. Although the midline remained heavily labeled, significantly fewer processes were detected in the mantle at E12, including the area around NL [Fig. 2(E,F)]. Few fibers extended radially at this age, reflecting either a decrease in vimentin expression or the retraction of vimentin-positive fibers.

At E12–13, EphA4 labeling was found in the dorsal and ventral neuropil regions of NL, but not in NM [Fig. 2(F)]. Fine vimentin-positive processes were distributed along the dorsal neuropil of NL, although no coexpression was detected between vimentin processes and EphA4 [Fig. 2(F)], consistent with the observation that EphA4 expression is limited to NL cell bodies and dendrites (Cramer et al., 2000b). Brain-

Figure 2 Vimentin and EphA4 expression in the auditory brainstem from E6 to E12. A: Long radial processes extend from cells in the ventricular zone (black boxes in VZ, see inset 1 and 2) to the pial surface of the brainstem at E6. The midline contains a dense population of vimentin-labeled processes (long black arrow). Note that the auditory anlage (AA) is devoid of any vimentin immunolabeling. Several fascicles of vimentin-positive processes can be observed throughout the brainstem (short black arrows). B: EphA4 (red) and vimentin (green) show extensive coexpression at E7. The medial region of the brainstem proximal to the midline contains vimentin-positive processes (long white arrow) but not EphA4. The majority of coexpression occurs in the ventral radial extensions (short white arrows), but not the area in contact with the pial surface. C: At E8, few fascicles of vimentin processes are observed. Expression in the VZ has also decreased, although some cell bodies can still be detected (black boxes). The auditory anlage remains devoid of vimentin labeling. The midline remains intensely labeled (long black arrow). D: At E10, vimentin-positive processes are intercalated among the neurons of NM and NL at the dorsal margins adjacent to cell bodies in each nucleus (white arrows). Vimentin-positive fibers located in the ventral portion of NL run parallel to the mediolateral axis of the nucleus (white arrowheads). E: At E12, some processes remain throughout both NM and NL (white arrows), including some that cross parallel to the mediolateral axis of the nuclei (white arrowheads). F: EphA4 and vimentin display little overlap in expression at E12. Vimentin processes that extend through NL (white arrows) do not express EphA4. Fine vimentin-positive processes are located within dorsal neuropil region of NL, which expresses EphA4. EphA4 is not expressed in NM, but numerous vimentin-positive processes are within the nuclei (white arrows) and parallel to NL (white arrowheads). In this and all micrographs, dorsal is up, ventral is down, medial is to the left, and lateral is to the right. Scale bars: (A–F) 50 μm, (A1, A2) 8 μm.

Figure 3 Polyclonal GFAP (pGFAP) labeling from E10 to E19. A: GFAP expression can first be detected at E10. Long processes extend from the contralateral side, cross the midline, and run ventrally along NL, parallel to the axis of the cell layer. Processes extend along the outer two-thirds of the cell layer. GFAP-labeled processes are also located in the area where VIIIth nerve afferents enter the brainstem (black arrow). Diffuse labeling is seen in the dorsolateral region to NM (white asterisk). Processes are seen crossing toward the midline (white arrows). B: Double immunolabeling for vimentin (green) and pGFAP (red) shows no coexpression at E10. Note that vimentin and pGFAP-labeled processes are differentially expressed along the glial margin of NL. Vimentin processes extend from the dorsal margin through the cell body layer to the ventral neuropil region (white arrows). Processes labeled with pGFAP are just outside the ventral neuropil (white arrowheads). C: E12 brainstems exhibit an increase in pGFAP-labeled processes; along mediolateral axis of NL, in the dorsolateral region adjacent to NM (white asterisks), and where VIIIth nerve afferents enter the brainstem (black arrowhead). There are several processes that extend out of NM toward the midline and some that cross through the most medial portion of NL (white arrows). D: At E14, labeled processes are located along the entire ventral mediolateral extent of NL and along the dorsal side of NL (white arrows). A few astrocytes are located in the ventral mantle and around the ventral margin of NL (yellow arrowheads). Processes remain along the pathway of VIIIth afferents (black arrow). E: At E16, pGFAP immunolabeling in processes has diminished. Stereotypical astrocytic bodies are seen along the ventral margin of NL, as well as further ventral in the mantle of the brainstem (yellow arrowheads). pGFAP-positive processes penetrate the NL cell layer and can be observed throughout NM (white arrows). F: High magnification of the NL cell layer demonstrates astrocytic processes (black arrows) entering into the cell layer from astrocytes that lie along the ventral neuropil in the glial margin (yellow arrowheads). Note the proximity of processes to the neurons of the NL monolayer. G: Stereotypical astrocytes found in the ventral glial margin of NL (yellow arrowheads) have processes that extend toward the cell layer (black arrowheads). H: At E19, astrocytes can be observed surrounding both NM and NL (yellow arrowheads). Both auditory nuclei contain GFAP-labeled processes (black arrows). Scale bars: (A, C–E, H) 100 μm, (B) 50 μm, and (F, G) 16 μm.

stem sections from embryos older than E14 contained little or no vimentin immunolabeling in this region.

Polyclonal and Monoclonal GFAP

Embryonic Days 10–13. Expression of GFAP was detected throughout the brainstem at E10–12 using a polyclonal antibody raised in rabbit (pGFAP; Fig. 3). GFAP-positive processes were densely packed and were not characteristic of fibrous astrocytes [Fig. 3(A–C)]. At E10, long processes extended from the midline and from the area just lateral to the contralateral NM [Fig. 3(A), white arrows]. The pGFAP-positive processes were present on the ventral side of NL and coursed parallel to the mediolateral axis of NL [Fig. 3(A)]. A dense tract of fibers was located along the medial third of NL, appearing as a 50–70 μm thick bundle, and tapering toward the most lateral point of NL, at which point individual processes could be distinguished. Although both vimentin and GFAP were expressed around NL, the two populations did not colocalize [Fig. 3(B)]. Although vimentin-positive fibers were observed ventral to NL were more abundant ventral to NL. This expression pattern indicates that distinct glial cell types form the dorsal versus ventral glial margins around NL.

By E12, the bundled processes expanded laterally to include at least two-thirds of the length of the NL cell layer [Fig. 3(C)] and were restricted to the ventral neuropil region around NL. Although some processes were detected dorsal to NL in close proximity to NM, they projected ventrally and toward the midline [Fig. 3(C,D), white arrows]. At these early ages, GFAP-positive processes did not seem to interact extensively with the ipsilateral NL. We found that at E10–E14 there were 6.0 $\pm$ 0.9 (mean $\pm$ s.e.m; $n = 12$ embryos) fibers crossing the NL cell body layer per section.

Embryonic Days 14–16. Expansion of pGFAP-immunolabeled processes continued from the medial to lateral extent of NL until about E14 [Fig. 3(A,C,D)], when processes extended along the entire mediolateral extent of NL [Fig. 3(D)]. The majority of labeled processes was observed along the ventral neuropil, although some were located in the most medial portion of the dorsal region of the NL cell layer [Fig. 3(D), white arrows].

Although astrocytic bodies could be found in E15 tissue, they were most easily detected in E16 brainstems [Fig. 3(E–G), yellow arrows]. In some brainstems, astrocytes were found far ventral to NL [Fig. 3(E)]. Fibrous astrocytes were identified by their stereotypical small somata with irregular projecting processes [Fig. 3(G)]. The majority of the cell bodies that were labeled for pGFAP were located in the ventral neuropil region around NL. High magnification images show that astrocytes were located ventral to neuropil [Fig. 3(F,G)].

Expression of GFAP was more prevalent in the dorsolateral region adjacent to NM [Fig. 3(E), asterisk]. Some of these processes projected ventrally toward the dorsal neuropil region of NL. Other processes traversed medially into NM, appearing to terminate around individual cells [Fig. 3(E)]. By E16, the long pGFAP-positive processes appeared less prominent as astrocytic cell bodies and processes became more evident [Fig. 3(E)].

When examining NL at high magnification, we found that there were a number of processes that were intercalated through the cell layer [Fig. 3(E), white arrows; 3(F), black arrows]. Careful examination of the astrocyte cell bodies surrounding NL revealed that they were the source of thin processes that penetrated the cell layer [Fig. 3(G), black arrowheads] and in some cases appeared to extend dorsally from the ventral margin, then terminate in close proximity to neuronal somata [Fig. 3(F), black arrows].

The change in GFAP expression pattern from long fibers to astrocytic cell bodies might reflect that the polyclonal antibody labels distinct populations of glia at different ages. To test this hypothesis, we used a second, monoclonal antibody to recognize GFAP expression. This mGFAP revealed no immunolabeled cells or processes until E15 [Fig. 4(A)]. This age coincided with a decrease in the axonlike processes and an emergence of stereotypical astrocytic bodies. Astrocytes labeled with mGFAP were found in the same location as those that were observed with pGFAP (yellow arrowheads in Fig. 4). Processes labeled with mGFAP penetrated the NL cell layer at E16 [Fig. 4(B,C), black arrows]. We found that at ages E15 and older there were 24.8 $\pm$ 3.0 such fibers per section, significantly greater than the number we observed in embryos younger than E15 ($p < 0.0001$, Student's t test). This finding suggests that these mGFAP-positive glial fibers interact with NL cells when the pathway is relatively mature. Expression based on mGFAP was localized to the ventral portion of NL; however, as with pGFAP, some processes were observed in the medial dorsal neuropil region around NL [Fig. 4(B,D), white arrows]. Similar to pGFAP at E16, mGFAP labeled cell bodies and processes originating from the dorsolateral area adjacent to NM at both E15 and E16 [Fig. 4(A,B)].

Embryonic Days 17–19. Astrocytes were located around NL, as well as in nonauditory areas (data not

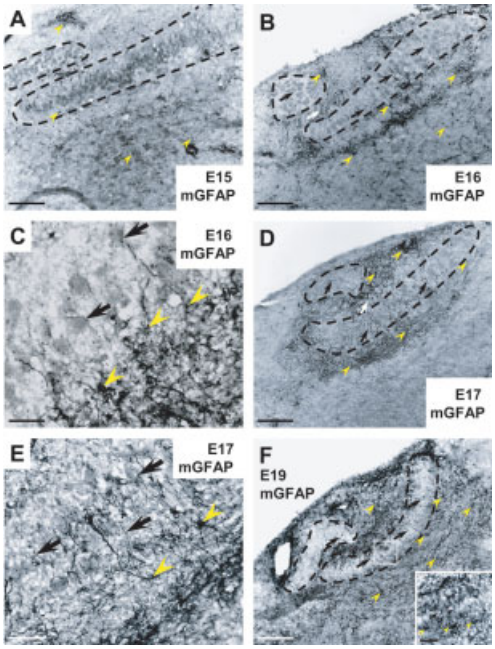

Figure 4 Expression of monoclonal GFAP throughout the brainstem starting at E15 and continuing to E19. A: mGFAP expression is first detected at E15. At this age, astrocytes are immunolabeled near NM, along the ventral glial margin of NL, and further ventral in the mantle (yellow arrowheads). B: There is an overall increase in expression of GFAP at E16. The majority of the astrocytes are located along the ventral glial margin of NL, although some are located lateral to NM and further ventral to NL (yellow arrowheads). Labeled processes extend into the cell layer, but do not appear to pass through (black arrows). Few labeled processes are seen passing into NM (black arrows). Some processes are observed in the dorsal, medial most portion of NL, but do not cross into the cell layer (white arrow). C: High magnification shows that the processes extending into NL are directly apposed to neurons in the NL cell body layer (black arrows). A number of astrocytes can be observed in the ventral glial margin of NL (yellow arrowheads). D: Noticeably, more astrocytes are immunolabeled at E17 (yellow arrowheads). Both dorsal and ventral margins of the NL cell layer contain labeled processes. There is also a notable increase in labeled processes that extend into NM and NL (black arrows). More labeled processes are observed in the dorsal, medial portion of NL than at earlier ages (white arrowhead). E: A high magnification image of NL at E17 reveals an intricate interaction between the GFAP-labeled processes and neurons in NL with processes appearing from both the dorsal and ventral sides around NL (black arrows). F: At E19, both nuclei are surrounded by a dense plexus of astrocytes (yellow arrowheads) and their processes pass into each respective cell layer (black arrows). This is an adjacent section to 3H, and the expression of GFAP is virtually identical. Scale bars: (A, B, D, F) 100 μm, (E) 25 μm, (C) 16 μm, and (F inset) 8 μm.

shown). pGFAP and mGFAP displayed similar, if not identical immunolabeling at these ages [compare adjacent sections; Figs. 3(H) and 4(F)]. In particular, long processes were no longer seen at these late embryonic ages. Multiple GFAP-expressing processes were observed and were densely packed throughout the NL cell layer [Figs. 3(H) and 4(D,F)], projecting both from the ventral neuropil and from the dorsal side of NL. In contrast with younger tissue, GFAP expression in older embryos was symmetrical about NL [Fig. 4(F)].

Expression in the population of cells adjacent to NM increased, becoming a dense conglomeration of processes and cell bodies, many of which appeared to be in close proximity to the VZ. Additionally, many labeled processes projected into NM, in close apposition to individual neurons. Neurons were often observed to have a thin GFAP-positive fiber surrounding the soma [Fig. 4(E), see high magnification inset in Fig. 4(F)]. Examination of the auditory nuclei at E19 revealed a highly structured arrangement of glial cell bodies and processes [Figs. 3(H) and 4(F)].

FluoroMyelin

Embryonic Days 10–13. We used a selective lipophilic myelin stain, FluoroMyelin (FM), to determine when myelin appears in the auditory circuit. FM and the previously described pGFAP were noted to have a similar spatiotemporal progression around NL from E10 to E19. Very little, if any, distinctive FM labeling was observed at E10 [Fig. 5(A)]. Only a few processes could be distinguished at E12 (data not shown), and occasional labeling was limited to the rostral portion of the auditory nuclei.

Embryonic Days 14–16. There was a substantial increase in FM labeling from E12 to E14, which included the expansion of labeling from the medial to lateral regions around NL. Unlike the asymmetric distribution of pGFAP-labeled processes along the ventral neuropil region of NL, FM was distributed on both the ventral and dorsal sides of NL, consistent with known axon trajectories [Fig. 5(C)] (Sanders, 1929; Young and Rubel, 1986).

In E16 tissue, FM-positive processes were found along the entire length of NL. Most labeling extended to at least two-thirds of NL along the ventral margin [Fig. 5(E)]. Processes in the dorsal half fanned out in a radial pattern and appeared to contact the most medial and lateral portions of NL. Processes were also present in NM, among the cell bodies [Fig. 5(E)]. Some FM labeling could be seen ventral to

NL; this area includes afferents of the VIIIth cranial nerve. Few processes were seen to extend beyond the neuropil region into the cell layer.

Embryonic Day 17–19. The overall density of labeling increased in the later stages of embryonic development. Labeled processes extended along the entire length of NL and within NM [Fig. 5(G)]. A group of processes extended from the ventral half of the brainstem [Fig. 5(G), white arrows]. These fibers might include inhibitory projections to NL arising from the superior olivary nucleus (SON) (Yang et al., 1999) or afferents projecting away from NL. In NL, 27.3 $\pm$ 7.5 FM-labeled fibers ($n = 3$) penetrated the NL cell layer per section, which was significantly greater than the number observed at E10-15 (5.5 $\pm$ 1.2; $n = 4$; $p < 0.05$), likely reflecting the increase in myelination of auditory axons at this age. At E19, there was an elaborate staining pattern with processes extending ventrally and dorsally along the entire extent of NL and into NM.

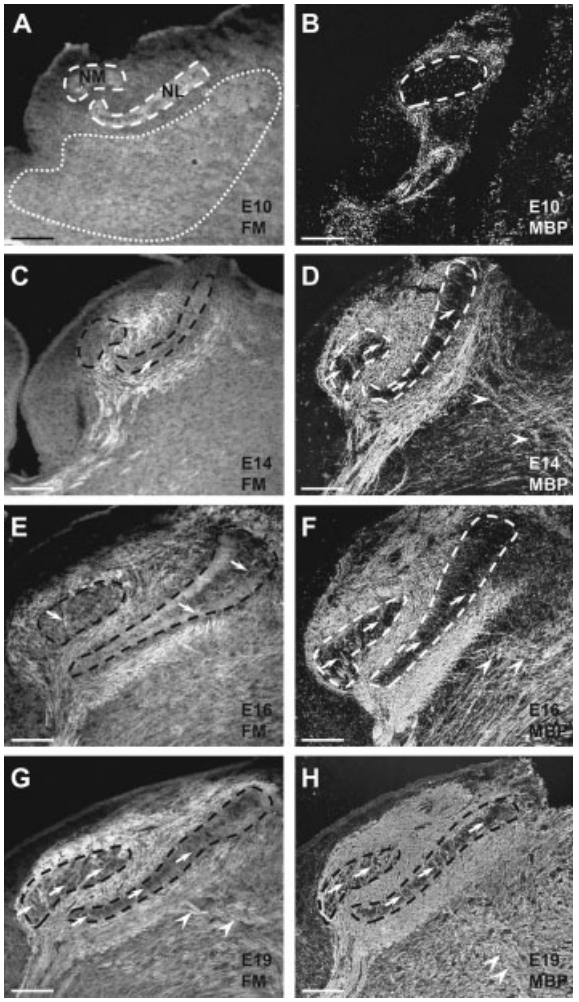

Myelin Basic Protein

Embryonic Days 10–13. Similar to FM labeling, MBP immunolabeling showed low levels from E10 to 12. Labeled processes were restricted to the rostral portion of the brainstem [Fig. 5(B)]. MBP-positive processes extended out from NM, crossed the midline, and passed through an area just ventral to NL. Ipsilateral processes were also seen extending towards the dorsal side of NL.

Embryonic Days 14–16. The density of labeled processes increased, resulting in much more intense labeling around NM and NL [Fig. 5(D,F)]. Almost the entire length of NL appeared to have labeled processes, although the processes did have a tapered pattern, with the most lateral processes being individually distinguishable.

Figure 5 Progression of myelin from E10 to E19 with FluoroMyelin (FM) and MBP. A: No distinctive processes could be observed at E10. A general hue was observed throughout the entire brainstem indicating that the dye was labeling the lipid membranes of all cells (dotted area). B: The only processes that could be found to label with MBP were located in the most rostral portion of NM and NL. C: At E14, individual processes labeled with FM extended across the midline to ventral NL and projected radially between NM and the dorsal margin of NL. D: Similar to FM, processes were labeled on the dorsal and ventral side of NL. Some processes crossed into NM and NL (white arrows). Processes projecting from the ventral portion of the brainstem were also labeled and may include afferents from the superior olivary nucleus (SON) (white arrowheads). E: A subtle increase in FM was observed at E16. Most notably, it appeared that there was a progression of myelin along the mediolateral axis of NL. Some labeled processes extended along the entire axis of the cell layer. At this age that FM processes were seen in NM and NL (white arrows). F: Many processes were labeled with MBP at E16, and these processes extended throughout NL. Many labeled processes were observed among the neurons of NM and NL (white arrows). Fibers between NL and the ventral brainstem were also labeled (white arrowheads). G: At E19, the entire length of NL was apposed by FM-labeled processes, several were also observed to penetrate the cell layer (white arrows). NM was surrounded by labeled processes, and several were observed to be within the nuclei (white arrows). Also, at E19, FM fibers in the ventral portion of the brainstem, similar to the pattern observed in younger tissue with MBP (white arrowheads). H: Both NM and NL were surrounded by MBP-labeled processes. Multiple processes extended into the nuclei (white arrows) and in ventral portions of the brainstem (white arrowheads), but the density of other ventral processes precluded identification of individual fibers. Scale bars: (A–H) 100 μm.

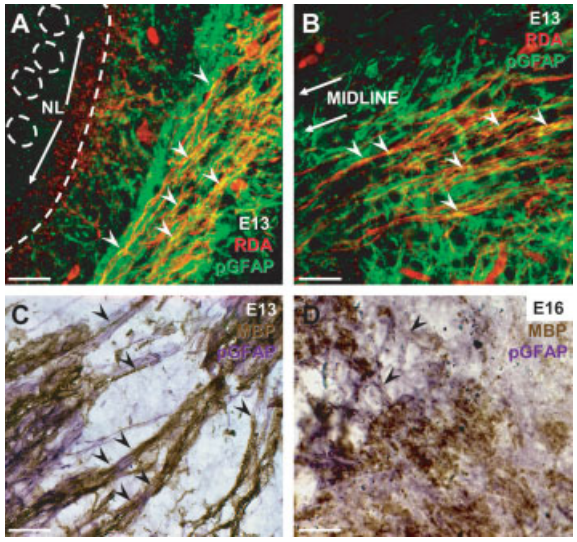

Figure 6 A, B: Association between rhodamine (RDA, red) labeled axons and pGFAP (green) processes at E13. C, D: pGFAP-labeled processes (purple) in apposition to MBP (brown) labeling at E13 and E16. A: Axons (red) from the contralateral NM project to the ventral neuropil of NL. The axons cross the glial margin that surrounds NL and synapse among dendrites of NL neurons. Note that GFAP processes do not cross the glial margin (white dashed line). We observed numerous locations where pGFAP and RDA colocalized or overlapped (white arrowheads). B: Near the midline pGFAP processes were observed in close proximity to RDA labeled axons. As with the axons that cross ventrally to NL, there were numerous locations of overlap or contact between the two processes (white arrowheads). C: At E13 axons that cross ventrally to NL have pGFAP and MBP processes that are directly apposed to one another on the axon, but do not overlap (black arrowheads). D: By E16, the distinction between pGFAP and MBP is not clear. Few pGFAP processes remain in direct apposition to MBP-labeled axons. Scale bars: (A–D) 16 μm.

At E14, the area surrounding NM was filled with an array of labeled processes [Fig. 5(D), white arrows]. Some processes were labeled within NM and could be followed dorsally to the ipsilateral NL. Multiple processes were observed within the NL cell body layer. Several axons that had their long axis through the coronal plane were observed in the dorsal and ventral regions around NL. Processes projecting from the ventral half of the brainstem were likely labeled axons projecting from the superior olive nucleus [Fig. 5(D), white arrowheads].

We observed an average of 42.6 $\pm$ 5.8 MBP-labeled processes per section ($n = 3$) penetrating NL in embryos E15 and older. Consistent with our data from FM labeling, this value was significantly greater than that seen in embryos at E10–14 (8.6 $\pm$ 5.9; $n = 3$; $p < 0.01$). By E16, the intensity of labeling was very high [Fig. 5(F)]. The areas dorsal and ventral to NL were filled with MBP-labeled processes. MBP labeling was seen throughout the areas where VIIIth nerve afferents enter the brainstem and where both auditory and vestibular nuclei are located.

MBP had a similar expression pattern to pGFAP at the ages before E16 [compare Fig. 3(A,C) with Fig. 5(D,F)]. Double-immunolabeling experiments were performed to determine the spatial relationship between the two proteins. Labeling in the ventral portion of NL revealed little coexpression. However, the two antibodies recognized antigens that were directly apposed along individual processes [Fig. 6(C), black arrowheads]. At E16, MBP labeling had increased and the fewer pGFAP processes were observed to be in apposition to MBP labeling [Fig. 6(D)].

Embryonic Days 17–19. The entire extent of NL contained labeled processes, and individual fibers were difficult to distinguish. NM neurons were surrounded by MBP labeling. In some cases, processes were found between neurons in the NL single cell layer. Both dorsal and ventral aspects of the brainstem contained labeled fiber tracts. In some of the less dense areas, axons could be seen crossing through the coronal plane as observed at younger ages.

Rhodamine Labeling. Although pGFAP appeared to specifically recognize GFAP on the Western blot, we were concerned that the appearance of pGFAP-labeled processes in proximity to the NL cell layer was due to cross-reactivity in the tissue between the pGFAP antibody and neuronal proteins. To evaluate this possibility, we injected rhodamine dye (RDA) into NM or the midline. Confocal images displayed some overlap with pGFAP; however, it did not appear that the RDA axons were themselves expressing GFAP [Fig. 6(A,B)]. Figure 6(A) shows that while RDA-labeled axons penetrated into the cell layer before E15, pGFAP processes did not [Fig. 6(A)]. Image stacks confirmed that pGFAP processes appeared to be in close apposition with and often envelop the full diameter of the RDA labeled axon.

DISCUSSION

Our results demonstrate that distinct glial populations exist throughout the auditory brainstem, and the proteins that identify these populations appear in specific temporal sequence throughout embryologic development. Anatomically, the data are consistent with findings that glia are often found in close proximity to neurons throughout maturation. Moreover, we find

that our results coincide with characteristic changes that are critical for functional auditory brainstem circuitry. These correlations suggest a role for glia in the development of the auditory circuit.

Vimentin-Positive Processes Are in Close Proximity to Neurons in NM and NL

In the avian brain, neurons have been observed to migrate along long vimentin-positive radial processes until they reach their destination and differentiate (Alvarez-Buylla et al., 1987; Alvarez-Buylla and Nottebohm, 1988). Previously, we suggested that the expression of EphA4 in the brainstem prior to the differentiation of nuclei may be related to the migration of neurons to their target destination (Cramer et al., 2000b). At E6, when the nuclei have yet to become differentiated, the anlage is completely devoid of vimentin-positive radial fibers. EphA4 exhibits a similar distribution and pattern as that of the vimentin-positive processes, which suggest a potential role for neuroglial interactions. We observed coexpression of EphA4 and vimentin in a subset of radial processes, specifically those whose processes extend across the dorsomedial portion of the mantle. This colocalization may be indicative of a role for EphA4 in neuroglial interactions in other brainstem nuclei. EphA4 is expressed in a specialized astroglial population in the optic nerve head at a time when retinal ganglion cell axons pass through the optic chiasm (Petros et al., 2006). Therefore, our data are consistent with a role for EphA4 in early developmental plasticity.

It is possible that similar to other brainstem nuclei, postmitotic neurons of NM and NL migrate to their respective positions via neurophilic migration, making use of axon fiber tracts (Rakic, 1990). This type of neuronal migration allows for tangential movement, without requiring contact with radial fibers. Book and Morest observed the formation of NM via perikaryal translocation of precursors from the anlage (1990). Therefore, it was surprising to find that at E10 a dense plexus of vimentin processes among the neurons of NM and NL. Perhaps similar to Cajal-Retzius cells found in the mammalian dorsal cochlear nucleus, these processes are responsible for the laminar arrangement of neurons in NL, but not the initial migration from the anlage (Takaoka et al., 2005).

Between E10 and E13, we observed fine vimentin processes throughout the entire extent of NL, with the majority populated in the dorsal neuropil. Although we observed no coexpression between the vimentin processes and EphA4 in the dorsal neuropil (Cramer et al., 2000b) at these ages, the overlapping domains of expression suggests that some interaction exists between vimentin-positive processes and EphA4-expressing dendrites. A number of studies have suggested a role for EphA4 in spine morphology and found that spines retracted when EphA4 was activated by a ligand on an axon terminal or glial process (Murai et al., 2003; Fu et al., 2007; Tremblay et al., 2007). Although the dendrites in NL are aspiny, glia may nonetheless play a corresponding role in the maturation of these auditory synapses.

Physiological postsynaptic responses are first detected between E11 and E13 in the chick auditory brainstem (Jackson et al., 1982). A recent study suggests that the window for the development of NM synapses is between E9 and E14 (Hendricks et al., 2006). Specifically, the synaptic vesicle protein SV2 becomes localized to the cell bodies at E12. Vimentin labeling begins to diminish, but remains in NM and in some limited fashion in the dorsal NL neuropil. Taken together, the data suggest that the vimentin processes may play a role facilitating maturation at this stage of development.

Astrocytes Located Around NL Display Highly Integrated Processes That Penetrate the Cell Layer

At E15, both the monoclonal and polyclonal antibodies to GFAP recognized a similar epitope, labeling astrocytic bodies and their associated processes. Previous studies have identified glia around NL either by thionin labeling, in ultrastructural analysis following deafferentation, or by labeling for an astrocyte-specific K^+ channel (Lippe et al., 1980; Deitch and Rubel, 1989; Feng and Morest, 2006). Our observation that GFAP processes project into NL during development provides further support for multiple roles of astrocytes in the development and maintenance of synapses in auditory system.

Previous studies have reported that vimentin-positive glia transition into GFAP-expressing astrocytes (Pixley and de Vellis, 1984). We sought to determine whether these astrocytes were derived from vimentin-expressing radial glia, however, vimentin expression was no longer observed by E13, while GFAP-expressing astrocytes do not appear until E15. No coexpression of vimentin and GFAP was observed at E13. Some studies have reported an intermediate phenotype between radial glia and astrocytes (Jing et al., 2007); however, our data suggest these two populations of glia do not appear anatomically or phenotypically related in the auditory brainstem. Although the data suggest that vimentin-positive glia may contribute minimally to the dorsolateral population of

GFAP-expressing astrocytes, the primary role is still undetermined.

Starting at E15, NL dendrites undergo structural modifications that establish a medial to lateral gradient of dendritic arbor size (Smith, 1981). As a result, anteromedial dendrites are shorter and closer to the cell body, while caudolateral dendrites are longer and distal from the NL cell body. This gradient optimizes the ability of neurons to detect coincidence at best frequencies, reducing jitter even as simulation frequency increases (Smith and Rubel, 1979; Agmon-Snir et al., 1998). Although afferent activity may be sufficient to regulate the reorientation of the dendritic gradient, additional communication must exist to coordinate reorganization across the dorsal to ventral extent of the nucleus. At E15, GFAP-immunolabeled astrocytes and their processes penetrate the neuropil and the glial margin around NL begins to migrate toward the cell layer. These observations are consistent with a role in developing the structure of NL and possibly facilitating the architecture of synaptic connections. Similar to the way Bergmann glia provide a scaffold and molecular signaling in the development of the dendritic arbors of Purkinje cells in the cerebellum, astrocytes that surround NL may aid in the patterning of dendritic arbors (Bellamy, 2006; Slezak et al., 2006). There may also be some molecular similarities in the way cerebellar dendrites and auditory dendrites elaborate and form their characteristic patterns (Lin et al., 2001).

Recent work has highlighted the "tripartite synapse," suggesting that glial cells act as the third member of the synapse, arbitrating between neurons (Araque et al., 2001; Halassa et al., 2007). In addition to supplying necessary signaling for excitatory synapses, astrocytes have been shown to modulate the formation of inhibitory synapses via TrkB signaling in cultured hippocampal neurons (Elmariah et al., 2005).

In the chick auditory brainstem, TrkB receptors are expressed in the ventral neuropil of NL throughout development (Cochran et al., 1999), supporting a relationship with astrocytes that are located primarily ventral to NL. Before the detection of hyperpolarizing current, $GABA_B$ subunits are located in the somatic regions of NL neurons (Burger et al., 2005b). It is not until E15 that these subunits form a heterodimer and migrate to the cell surface and become functional (Calver et al., 2002; Burger et al., 2005b). One possibility is that astrocytes are responsible for recruiting $GABA_B$ subunits to the surface.

This ongoing effort to identify astrocyte-derived molecules that allow for signaling between neurons and astrocytes requires that we determine whether astrocytes are present during particular stages of development (Mauch et al., 2001; Christopherson et al., 2005; Colon-Ramos et al., 2007). The present data show the progression of astrocytes in the auditory pathway. Further studies are needed to determine whether and how this signaling occurs during development in these auditory nuclei and to identify signaling molecules.

FM and MBP Complement Each Other During Myelinogenesis in the Developing Avian Auditory Nuclei

We found that myelinated axons could be distinguished as early as E11, which is after axons have reached their target and topographic organization is complete in NL (Young and Rubel, 1986). The appearance of myelinated axons follows the onset of activity in NM and NL, starting with those axons in the most medial portion of NL and continuing along the mediolateral axis (Jackson et al., 1982). The threshold to evoke response in NL decreases significantly ($\sim$43%) from E12 to E19 (Saunders et al., 1973). This is the same time which we see an increase in myelinated axons. This trend may indicate a role for myelin in the synchronization of firing by facilitating an increase in conduction velocity with a maturing circuit. Our results are consistent with a recent study, which described in detail the onset of myelination in the barn owl (Cheng and Carr, 2007), in which myelin appears after the formation of synapses and therefore may act to stabilize the delay lines.

We sought to confirm our results with an antibody to MBP. The two labeling patterns were virtually identical, with subtle differences. It appears that the FM accumulation is delayed just slightly following the expression of MBP. Therefore, our results demonstrate that the progression of myelination starts about E10 and continues to a mature state just before hatching (E21). Our results are also consistent with previous western-blot analysis of MBP in the developing chick (Macklin and Weill, 1985).

Few studies have attempted to define the window in which myelination occurs in the chick (Rodriguez and Rebollo, 1966; Hartman et al., 1979; Macklin and Weill, 1985), but none have examined the progression of myelin during embryogenesis in NM and NL. The results from the present experiments address a basic question; does the spatiotemporal distribution of myelin support a role for the inhibition of outgrowth during development? The timing of expression suggests that rather than affecting the initial wiring, myelin acts to maintain an established circuit (Schwegler et al., 1995; Phokeo et al., 2002; Aloy et al., 2006).

Polyclonal GFAP Labels Novel Population of Glia

Although the pGFAP antibody did not cross-react with neurofilament or traced axons, its appearance from E10 to E14 included long axonlike processes. This pattern is consistent with an interaction between glial cells and axons. Similar pGFAP labeling was described by Pecchi et al. in the nucleus tractus solitarius in the rat as radial-glia-like cells (2007). They offered the possibility that the GFAP-labeled glia were involved with progenitors in the subventricular zone. Our evidence suggests a more direct interaction with axons.

Rhodamine (RDA) labeling revealed some colocalization with pGFAP, which could indicate locations of contact. Although axons labeled with RDA enter the NL cell layer, the pGFAP-labeled processes do not. This result is consistent with what we observed for MBP at younger ages and provides evidence to suggest that pGFAP labels a population of oligodendrocytes from E10 to E14.

Indeed, premyelinating oligodendrocytes have been shown to express GFAP before becoming mature oligodendrocytes (Casper and McCarthy, 2006). Type-2 astrocytes that express GFAP also express A2B5, which is a ganglioside also expressed in oligodendrocyte progenitors (Compston et al., 1997; de Castro and Bribian, 2005). To further test this possibility that pGFAP labels immature oligodendrocytes, we labeled for MBP and pGFAP at an age when individual GFAP-positive processes could be discerned. The pattern revealed a complementary overlap, but not coexpression, indicating that it is possible that pGFAP labels an epitope of an intermediate filament protein found in oligodendrocytes before their expression of MBP. Future studies should label with additional putative oligodendrocyte markers or perform a rigorous ultrastructural analysis to confirm these findings.

The ontogeny of the avian auditory circuit is well-characterized, and the physiological and anatomical events that lead to the functioning circuit are well established. Here, we described our observations on glial cell types in the context of these developmental events. We found a strong correlation between glial maturation and circuit formation. Functional studies will be needed to characterize the roles of glia in the formation of these pathways.

The authors thank Dr. Elena Pasquale for providing the EphA4 antibody, Dr. Susana Cohen-Cory and Margarita Meynard for assistance with the confocal microscope, and Lan Li for technical assistance. We thank Dr. Candace Hsieh, Christine Charvet, and Nicole Shirkey for helpful comments on the manuscript.

REFERENCES

Agmon-Snir H, Carr CE, Rinzel J. 1998. The role of dendrites in auditory coincidence detection. Nature 393: 268–272.

Aloy EM, Weinmann O, Pot C, Kasper H, Dodd DA, Rulicke T, Rossi F, Schwab ME. 2006. Synaptic destabilization by neuronal Nogo-A. Brain Cell Biol 35:137–156.

Alvarez-Buylla A, Buskirk DR, Nottebohm F. 1987. Monoclonal antibody reveals radial glia in adult avian brain. J Comp Neurol 264:159–170.

Alvarez-Buylla A, Nottebohm F. 1988. Migration of young neurons in adult avian brain. Nature 335:353–354.

Araque A, Carmignoto G, Haydon PG. 2001. Dynamic signaling between astrocytes and neurons. Annu Rev Physiol 63:795–813.

Bellamy TC. 2006. Interactions between Purkinje neurones and Bergmann glia. Cerebellum 5:116–126.

Bergles DE, Diamond JS, Jahr CE. 1999. Clearance of glutamate inside the synapse and beyond. Curr Opin Neurobiol 9:293–298.

Book KJ, Morest DK. 1990. Migration of neuroblasts by perikaryal translocation: role of cellular elongation and axonal outgrowth in the acoustic nuclei of the chick embryo medulla. J Comp Neurol 297:55–76.

Burger RM, Cramer KS, Pfeiffer JD, Rubel EW. 2005a. Avian superior olivary nucleus provides divergent inhibitory input to parallel auditory pathways. J Comp Neurol 481:6–18.

Burger RM, Pfeiffer JD, Westrum LE, Bernard A, Rubel EW. 2005b. Expression of GABA(B) receptor in the avian auditory brainstem: Ontogeny, afferent deprivation, and ultrastructure. J Comp Neurol 489:11–22.

Calver AR, Davies CH, Pangalos M. 2002. $GABA_B$ receptors: From monogamy to promiscuity. Neurosignals 11:299–314.

Carr CJ. 1991. Regulatory implications of chronotoxicology and chronopharmacodynamics. Ann NY Acad Sci 618:558–562.

Carr CE, Konishi M. 1990. A circuit for detection of interaural time differences in the brain stem of the barn owl. J Neurosci 10:3227–3246.

Casper KB, McCarthy KD. 2006. GFAP-positive progenitor cells produce neurons and oligodendrocytes throughout the CNS. Mol Cell Neurosci 31:676–684.

Chen ZJ, Negra M, Levine A, Ughrin Y, Levine JM. 2002. Oligodendrocyte precursor cells: reactive cells that inhibit axon growth and regeneration. J Neurocytol 31:481–495.

Cheng SM, Carr CE. 2007. Functional delay of myelination of auditory delay lines in the nucleus laminaris of the barn owl. Dev Neurobiol 67:1957–1974.

Christopherson KS, Ullian EM, Stokes CC, Mullowney CE, Hell JW, Agah A, Lawler J, et al. 2005. Thrombospondins are astrocyte-secreted proteins that promote CNS synaptogenesis. Cell 120:421–433.

Cochran SL, Stone JS, Bermingham-McDonogh O, Akers SR, Lefcort F, Rubel EW. 1999. Ontogenetic expression of trk neurotrophin receptors in the chick auditory system. J Comp Neurol 413:271–288.

Colon-Ramos DA, Margeta MA, Shen K. 2007. Glia promote local synaptogenesis through UNC-6 (netrin) signaling in *C. elegans*. Science 318:103–106.

Compston A, Zajicek J, Sussman J, Webb A, Hall G, Muir D, Shaw C, et al. 1997. Glial lineages and myelination in the central nervous system. J Anat 190 (Part 2):161–200.

Cramer KS. 2005. Eph proteins and the assembly of auditory circuits. Heart Res 206:42–51.

Cramer KS, Bermingham-McDonogh O, Krull CE, Rubel EW. 2004. EphA4 signaling promotes axon segregation in the developing auditory system. Dev Biol 269: 26–35.

Cramer KS, Cerretti DP, Siddiqui SA. 2006. EphB2 regulates axonal growth at the midline in the developing auditory brainstem. Dev Biol 295:76–89.

Cramer KS, Fraser SE, Rubel EW. 2000a. Embryonic origins of auditory brain-stem nuclei in the chick hindbrain. Dev Biol 224:138–151.

Cramer KS, Rosenberger MH, Frost DM, Cochran SL, Pasquale EB, Rubel EW. 2000b. Developmental regulation of EphA4 expression in the chick auditory brainstem. J Comp Neurol 426:270–278.

de Castro F, Bribian A. 2005. The molecular orchestra of the migration of oligodendrocyte precursors during development. Brain Res Brain Res Rev 49:227–241.

Deitch JS, Rubel EW. 1989. Rapid changes in ultrastructure during deafferentation-induced dendritic atrophy. J Comp Neurol 281:234–258.

Elmariah SB, Oh EJ, Hughes EG, Balice-Gordon RJ. 2005. Astrocytes regulate inhibitory synapse formation via Trk-mediated modulation of postsynaptic GABAA receptors. J Neurosci 25:3638–3650.

Feng JJ, Morest DK. 2006. Development of synapses and expression of a voltage-gated potassium channel in chick embryonic auditory nuclei. Hear Res 216–217:116–126.

Fritzsch B, Pirvola U, Ylikoski J. 1999. Making and breaking the innervation of the ear: neurotrophic support during ear development and its clinical implications. Cell Tissue Res 295:369–382.

Fu WY, Chen Y, Sahin M, Zhao XS, Shi L, Bikoff JB, Lai KO, et al. 2007. Cdk5 regulates EphA4-mediated dendritic spine retraction through an ephexin1-dependent mechanism. Nat Neurosci 10:67–76.

Halassa MM, Fellin T, Haydon PG. 2007. The tripartite synapse: roles for gliotransmission in health and disease. Trends Mol Med 13:54–63.

Harkmark W. 1954. Cell migrations from the rhombic lip to the inferior olive, the nucleus raphe and the pons; a morphological and experimental investigation on chick embryos. J Comp Neurol 100:115–209.

Hartman BK, Agrawal HC, Kalmbach S, Shearer WT. 1979. A comparative study of the immunohistochemical localization of basic protein to myelin and oligodendrocytes in rat and chicken brain. J Comp Neurol 188:273–290.

Hendricks SJ, Rubel EW, Nishi R. 2006. Formation of the avian nucleus magnocellularis from the auditory anlage. J Comp Neurol 498:433–442.

Howell DM, Morgan WJ, Jarjour AA, Spirou GA, Berrebi AS, Kennedy TE, Mathers PH. 2007. Molecular guidance cues necessary for axon pathfinding from the ventral cochlear nucleus. J Comp Neurol 504:533–549.

Huffman KJ, Cramer KS. 2007. EphA4 misexpression alters tonotopic projections in the auditory brainstem. Dev Neurobiol 67:1655–1668.

Jackson H, Hackett JT, Rubel EW. 1982. Organization and development of brain stem auditory nuclei in the chick: Ontogeny of postsynaptic responses. J Comp Neurol 210:80–86.

Jhaveri S, Morest DK. 1982. Sequential alterations of neuronal architecture in nucleus magnocellularis of the developing chicken: a Golgi study. Neuroscience 7:837–853.

Jing R, Wilhelmsson U, Goodwill W, Li L, Pan Y, Pekny M, Skalli O. 2007. Synemin is expressed in reactive astrocytes in neurotrauma and interacts differentially with vimentin and GFAP intermediate filament networks. J Cell Sci 120:1267–1277.

Kapfhammer JP. 1997. Axon sprouting in the spinal cord: growth promoting and growth inhibitory mechanisms. Anat Embryol (Berl) 196:417–426.

Lin JC, Cai L, Cepko CL. 2001. The external granule layer of the developing chick cerebellum generates granule cells and cells of the isthmus and rostral hindbrain. J Neurosci 21:159–168.

Lippe WR, Steward O, Rubel EW. 1980. The effect of unilateral basilar papilla removal upon nuclei laminaris and magnocellularis of the chick examined with [3H]2-deoxy-D-glucose autoradiography. Brain Res 196:43–58.

Macklin WB, Weill CL. 1985. Appearance of myelin proteins during development in the chick central nervous system. Dev Neurosci 7:170–178.

Mauch DH, Nagler K, Schumacher S, Goritz C, Muller EC, Otto A, Pfrieger FW. 2001. CNS synaptogenesis promoted by glia-derived cholesterol. Science 294:1354–1357.

Murai KK, Nguyen LN, Irie F, Yamaguchi Y, Pasquale EB. 2003. Control of hippocampal dendritic spine morphology through ephrin-A3/EphA4 signaling. Nat Neurosci 6:153–160.

Overholt EM, Rubel EW, Hyson RL. 1992. A circuit for coding interaural time differences in the chick brainstem. J Neurosci 12:1698–1708.

Parks TN. 1981. Morphology of axosomatic endings in an avian cochlear nucleus: nucleus magnocellularis of the chicken. J Comp Neurol 203:425–440.

Pascual O, Casper KB, Kubera C, Zhang J, Revilla-Sanchez R, Sul JY, Takano H, Moss SJ, McCarthy K, Haydon PG. 2005. Astrocytic purinergic signaling coordinates synaptic networks. Science 310:113–116.

Pecchi E, Dallaporta M, Charrier C, Pio J, Jean A, Moyse E, Troadec JD. 2007. Glial fibrillary acidic protein (GFAP)-positive radial-like cells are present in the vicinity of proliferative progenitors in the nucleus tractus solitarius of adult rat. J Comp Neurol 501:353–368.

Pekny M, Pekna M. 2004. Astrocyte intermediate filaments in CNS pathologies and regeneration. J Pathol 204:428–437.

Petros TJ, Williams SE, Mason CA. 2006. Temporal regulation of EphA4 in astroglia during murine retinal and optic nerve development. Mol Cell Neurosci 32:49–66.

Phokeo V, Kwiecien JM, Ball AK. 2002. Characterization of the optic nerve and retinal ganglion cell layer in the dysmyelinated adult Long Evans Shaker rat: Evidence for axonal sprouting. J Comp Neurol 451:213–224.

Pixley SK, de Vellis J. 1984. Transition between immature radial glia and mature astrocytes studied with a monoclonal antibody to vimentin. Brain Res 317:201–209.

Poluch S, Juliano SL. 2007. A normal radial glial scaffold is necessary for migration of interneurons during neocortical development. Glia 55:822–830.

Rakic P. 1978. Neuronal migration and contact guidance in the primate telencephalon. Postgrad Med J 54 (Suppl 1): 25–40.

Rakic P. 1990. Principles of neural cell migration. Experientia 46:882–891.

Rodriguez MM, Rebollo MA. 1966. [Development of Corti's organ and the hearing duct in the chicken embryo. III. Cochlear nerve] An Fac Med Univ Repub Montev Urug 51:40–44.

Rubel EW, Smith DJ, Miller LC. 1976. Organization and development of brain stem auditory nuclei of the chicken: Ontogeny of *N. magnocellularis* and *N. laminaris*. J Comp Neurol 166:469–489.

Sanders EB. 1929. A consideration of certain bulbar, midbrain, and cerebellar centers and fiber tracts in birds. Philadelphia, PA: The Wistar Institute Press, pp 155–222. illus. 127 cm.

Sandvig A, Berry M, Barrett LB, Butt A, Logan A. 2004. Myelin-, reactive glia-, and scar-derived CNS axon growth inhibitors: Expression, receptor signaling, and correlation with axon regeneration. Glia 46:225–251.

Saunders JC, Coles RB, Gates GR. 1973. The development of auditory evoked responses in the cochlea and cochlear nuclei of the chick. Brain Res 63:59–74.

Schwegler G, Schwab ME, Kapfhammer JP. 1995. Increased collateral sprouting of primary afferents in the myelin-free spinal cord. J Neurosci 15:2756–2767.

Slezak M, Pfrieger FW, Soltys Z. 2006. Synaptic plasticity, astrocytes and morphological homeostasis. J Physiol Paris 99:84–91.

Smith DJ, Rubel EW. 1979. Organization and development of brain stem auditory nuclei of the chicken: dendritic gradients in nucleus laminaris. J Comp Neurol 186:213–239.

Smith ZD. 1981. Organization and development of brain stem auditory nuclei of the chicken: Dendritic development in *N. laminaris*. J Comp Neurol 203: 309–333.

Soans C, Holash JA, Pavlova Y, Pasquale EB. 1996. Developmental expression and distinctive tyrosine phosphorylation of the Eph-related receptor tyrosine kinase Cek9. J Cell Biol 135:781–795.

Takaoka Y, Setsu T, Misaki K, Yamauchi T, Terashima T. 2005. Expression of reelin in the dorsal cochlear nucleus of the mouse. Brain Res Dev Brain Res 159: 127–134.

Tierney TS, T PD, Xia G, Moore DR. 2001. Development of brain-derived neurotrophic factor and neurotrophin-3 immunoreactivity in the lower auditory brainstem of the postnatal gerbil. Eur J Neurosci 14:785–793.

Tremblay ME, Riad M, Bouvier D, Murai KK, Pasquale EB, Descarries L, Doucet G. 2007. Localization of EphA4 in axon terminals and dendritic spines of adult rat hippocampus. J Comp Neurol 501:691–702.

Webber A, Raz Y. 2006. Axon guidance cues in auditory development. Anat Rec A Discov Mol Cell Evol Biol 288:390–396.

Yang L, Monsivais P, Rubel EW. 1999. The superior olivary nucleus and its influence on nucleus laminaris: A source of inhibitory feedback for coincidence detection in the avian auditory brainstem. J Neurosci 19:2313–2325.

Young SR, Rubel EW. 1986. Embryogenesis of arborization pattern and topography of individual axons in *N. laminaris* of the chicken brain stem. J Comp Neurol 254:425–459.

Zhang JM, Wang HK, Ye CQ, Ge W, Chen Y, Jiang ZL, Wu CP, Poo MM, Duan S. 2003. ATP released by astrocytes mediates glutamatergic activity-dependent heterosynaptic suppression. Neuron 40:971–982.